

# Optimum distribution of steel slit-friction hybrid dampers based on life cycle cost

Mohamed Nour Eldin, Jaegoo Kim and Jinkoo Kim \*

Department of Civil and Architectural Engineering, Sungkyunkwan University, Suwon, Republic of Korea

(Received December 29, 2017, Revised February 22, 2018, Accepted April 4, 2018)

**Abstract.** This study investigated the seismic performance of a hybrid damper composed of a steel slit plate and friction pads, and an optimum retrofit scheme was developed based on life cycle cost. A sample hybrid damper was tested under cyclic loading to confirm its validity as a damping device and to construct its nonlinear analysis model. The effectiveness of the optimum damper distribution schemes was investigated by comparing the seismic fragility and the life cycle costs of the model structure before and after the retrofit. The test results showed that the damper behaved stably throughout the loading history. Numerical analysis results showed that the slit-friction hybrid dampers optimally distributed based on life cycle cost proved to be effective in minimizing the failure probability and the repair cost after earthquakes.

**Keywords:** steel slit dampers; friction dampers; seismic retrofit; optimum design; life cycle cost

## 1. Introduction

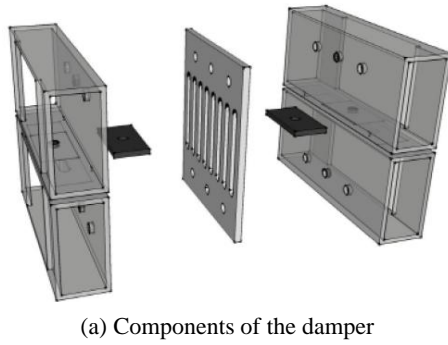
Simultaneous application of multiple energy dissipation mechanisms for seismic retrofit of existing structures has advantage in that multiple design objectives can be achieved by using multiple damping mechanisms. Many researchers have investigated the advantage of combined use of multiple devices. For example Tsai *et al.* (1998), Uetani *et al.* (2003), and Chen and Albermani (2008) studied combined displacement-dependent and velocity-dependent devices for seismic mitigation of structures to minimize the shortcomings of individual dampers. Marko *et al.* (2004) studied the effect of combined friction-viscoelastic damping devices strategically located within shear walls and demonstrated the feasibility of mitigating the seismic response of building structures by using embedded dampers. Marshall and Charney (2012) studied a hybrid system with buckling restrained braces and viscous fluid device by investigating the seismic response of steel frame structures. Optimum design procedures for hybrid or multiple dampers have been developed by Murakami *et al.* (2013). Xu *et al.* (2004, 2012, 2016) studied seismic performance and optimum design of hybrid damping mechanism including viscoelastic dampers. Lee and Kim (2015) investigated the effectiveness of a hybrid damper consisting of steel slit plate and rotational friction devices to be used effectively both for small and large earthquakes. Zahrai *et al.* (2015) studied the combined retrofit effect of using friction dampers and masonry infill panels. Lee *et al.* (2016) investigated the combined behavior of shear-type friction damper and non-uniform strip damper for multi-

level seismic protection. Xu *et al.* (2017) and Fan *et al.* (2017) developed a hysteretic energy dissipation bracing system combined with self-centering mechanism. Karunaratne *et al.* (2016) studied the effect of magneto-rheological and passive damper combinations for seismic mitigation of building structures. Sun *et al.* (2017) investigated the combined effect of added stiffness and hysteretic energy dissipation of a coupling beam. Zhan *et al.* (2017) developed a hybrid semi-active control device based on the super elastic properties of the shape memory alloy (SMA) and the inverse piezoelectric effect of piezoelectric (PZT) ceramics, and showed its effectiveness by mechanical properties test under different frequency and different voltage. Hessabi *et al.* (2017) explored the effects of tuned mass dampers on the seismic performance of structures with nonlinear base isolation systems. Lee *et al.* (2017) and Kim and Shin (2017) carried out seismic performance evaluation of a framed structure with different types of steel-friction hybrid dampers, and found that the seismic performances of the structure with the hybrid dampers are superior to that of the structure with individual dampers with the same yield strength. The results of the previous studies demonstrated the capability of hybrid passive systems to improve structural response compared with conventional lateral systems. The hybrid configuration improved some aspect of structural response providing benefits for multiple damage measures.

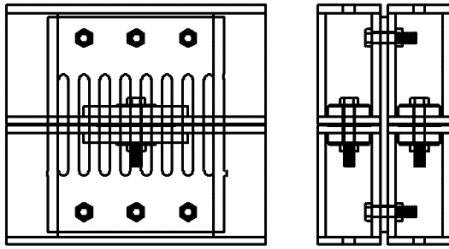
This study first investigated the seismic performance of a hybrid damper in which a steel slit plate and friction pads are combined to be used for seismic retrofit of a structure. A sample hybrid damper was tested under cyclic loading to confirm its validity as a damping device and to construct its nonlinear analysis model. Then optimal story-wise damper installation schemes were developed using genetic algorithm in such a way that the life cycle cost (LCC) of the retrofitted structure becomes minimum. For reducing

---

\*Corresponding author, Ph.D., Professor,  
E-mail: [jkim12@skku.edu](mailto:jkim12@skku.edu)



(a) Components of the damper



(b) Front and side views

Fig. 1 Configuration of the steel slit-friction hybrid damper

computation time required for LCC-based optimization of the damper installation, some simplification schemes were applied. The probabilities of reaching various damage states were obtained by fragility analysis to evaluate the margin for safety against earthquakes. The validities of the optimization schemes developed based on the minimum damper cost and on the minimum life cycle costs were compared.

## 2. A slit-friction hybrid damper considered

The hybrid damper developed in this study consists of a steel slit damper and two friction dampers connected in parallel as shown in Fig. 1. The advantage of the hybrid damper is that for small earthquakes only friction dampers are activated, while for large earthquakes both friction and slit dampers dissipate seismic energy. Both dampers can be easily manufactured by inexpensive materials such as friction pads, steel plates, and high tension bolts. The friction pads are inserted between two rectangular steel boxes, one of which is connected to the upper part of the slit plate and the other of which is connected to the bottom of the slit plate. The two rectangular steel boxes at both sides of the friction pad are fastened together by a high-tension bolt which goes through the slotted hole in the friction pad. The slip of friction pads occurs at small lateral displacement, which makes it effective in resisting small earthquakes and strong wind loads. The slit dampers remain elastic during small earthquakes and are activated at major earthquakes. In practice the slit plate is connected to the structure at both the top and bottom using very stiff steel trusses so that it deforms and dissipates hysteretic energy when inter-story drifts occur in the structure during seismic events. Rectangular plates are added to evenly distribute the clamping force from the bolt on the surface of the friction

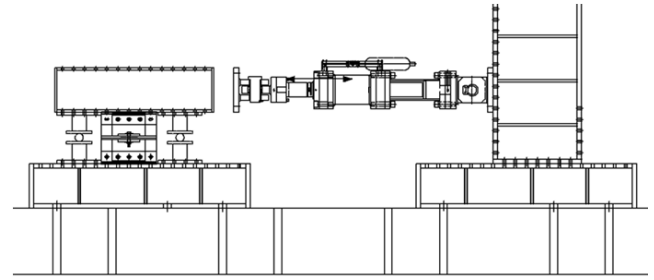


Fig. 2 Test setup for the hybrid damper



(a)



(b)

Fig. 3 Photographs of the steel slit-friction damper specimen

pad. The slit plate has 8 slit columns: the width, thickness, and the height of each slit column are 20 mm, 15 mm, and 200 mm respectively. The stiffness and yield strength of a slit damper can be derived as follows based on the assumption that the slit columns are fixed at both ends

$$k_s = n \frac{12EI}{l_o^3} = n \frac{Et b^3}{l_o^3} \quad (1a)$$

$$P_{ys} = \frac{2nM_p}{l_o} = \frac{nf_y t b^2}{2l_o} \quad (1b)$$

where  $n$  = number of strips,  $t$  = thickness of strips,  $b$  = width of strips, and  $l_o$  = length of the vertical strip. The yield force of the friction dampers,  $P_{yf}$ , is proportional to the clamping force,  $N$ , and the friction coefficient,  $\mu$ ; i.e.,  $P_{yf} = \mu N$ . The yield strength of the hybrid damper,  $P_{yh}$ , can be calculated by adding up those of the two individual dampers

$$P_{yh} = \mu N + \frac{nf_y t b^2}{2l_o} \quad (2)$$

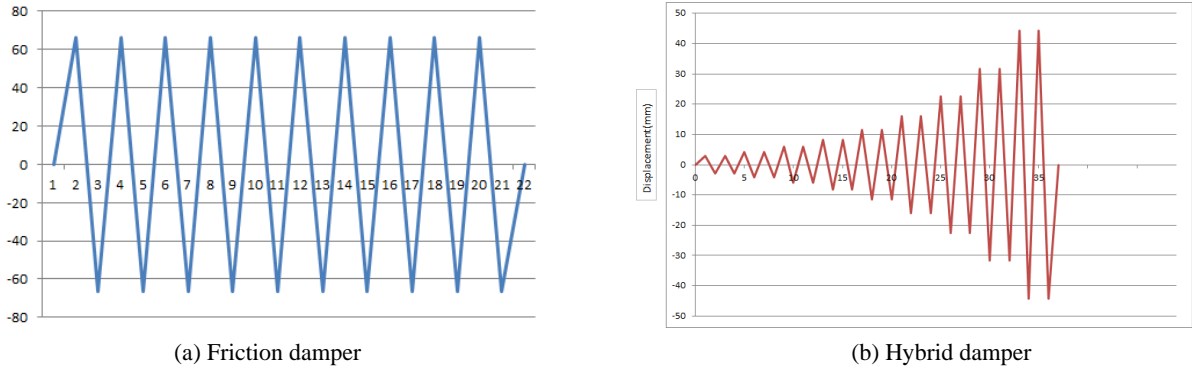


Fig. 4 Loading protocols used in the cyclic tests of the specimen

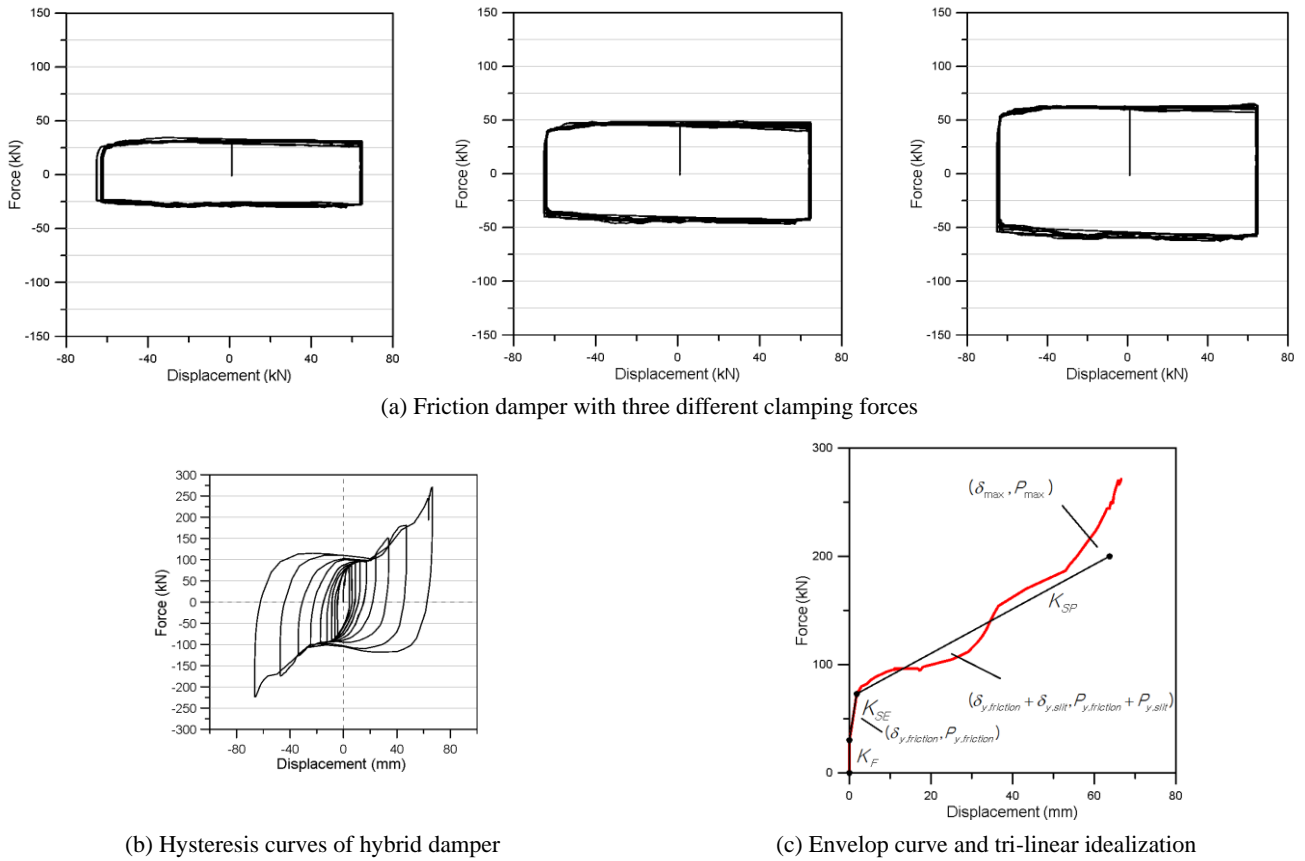


Fig. 5 Test results of the hybrid damper

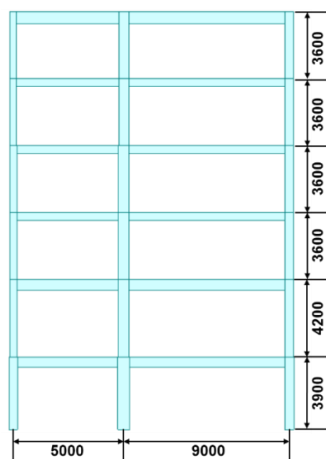
Displacement-controlled cyclic tests of the specimens were carried out using a 500 kN hydraulic servo actuator to evaluate the seismic performance of the hybrid damper. Fig. 2 depicts the test setup for the cyclic loading test, and Fig. 3 shows the photographs of the hybrid damper installed inside of the strong frame. The friction pads have dimensions of 150×80 mm with thickness of 4 mm, and the slit plate has overall dimension of 420×340×15 mm with the width and height of the slit columns 20×180 mm, respectively. The steel plate is made of SS400 steel with yield and ultimate strength of 320 and 400 MPa, respectively. The high-tension bolts used to provide clamping force on the friction pads have the tensile strength of 165 kN with diameter of 20 mm. LVDT (linear variable differential transformer) is

installed to measure the horizontal displacement of the specimens during experiments. Fig. 4 depicts the loading protocol used in the cyclic loading test of the specimen specified in the FEMA-461 (2007) for quasi-static cyclic loading tests.

Fig. 5(a) shows the test results of the friction damper with three different bolt clamping forces of 50, 75, and 100 kN. The tests were carried out by fixing the lower steel box to the strong frame and moving the upper steel box by the actuator. For the test of the friction damper 10 cycles of harmonic loading were applied in such a way that the maximum displacement of 65 mm is reached at each loading cycle. It also can be noticed that the friction damper generates almost identical rectangular hysteresis loops for

each loading cycle. Based on the slip force obtained from the test results and the bolt clamping force provided by the torque wrench, the friction coefficient  $\mu$  of the friction pads is determined to be approximately 0.6. In practice the proper slip force of the friction damper can be determined from preliminary analysis of the structure subjected to minor earthquakes (earthquakes with return period of 200 years, for example).

The yield force of the slit damper and the slip force of the friction damper are estimated to be 49 kN and 30 kN, respectively. This combination of two dampers results in yield strength of the hybrid damper of 79 kN. When the shear force imposed on the hybrid damper exceeds the slip force of the friction damper, the friction damper is activated and dissipates hysteretic energy while the slit damper remains elastic until the shear force reaches the combined yield strength of 79 kN. When the applied shear force reaches the combined yield strength of the hybrid damper, both the friction and the slit damper work together to dissipate seismic energy. At large lateral displacement a diagonal tension field is formed in the slit plate, which results in further increase of post-yield strength at lateral displacement higher than 30 mm as can be observed in the hysteresis curves depicted in Fig. 5. The envelop curve is idealized as three linear lines to be used as an analysis model as shown in Fig. 5(c). The slope of the second line obtained from the experiment, which is the stiffness of the slit damper, is 27.06 kN/mm. This value is slightly smaller than that of the slit damper computed from Eq. (1a), which is 32.53 kN/mm. The third line of the envelop curve, which is the post-yield stiffness of the damper, is 2.49 kN/mm. These are used as an analysis model in the nonlinear dynamic analysis of the structure retrofitted with the hybrid dampers. The increase in strength due to formation of tension field in steel hysteretic dampers can also be observed in Whittaker *et al.* (1991). AISC Seismic Provisions (2010) requires that the cumulative ductility ratio of a hysteretic device be larger than 200. In this study the cumulative ductility ratio of the hybrid damper turns out to be 295, which confirms that the damper has enough plastic deformation capability.



(a) Elevation view

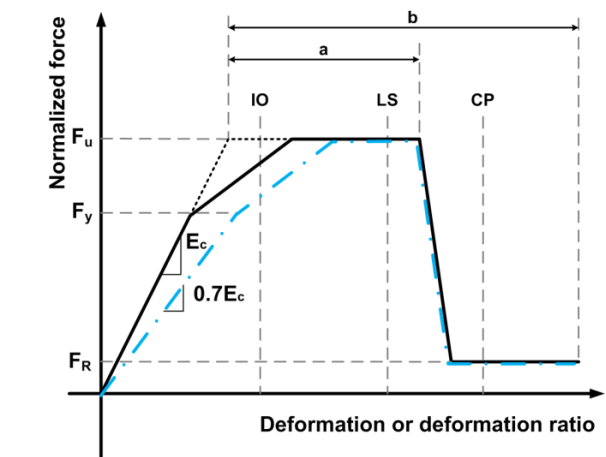


Fig. 7 Nonlinear model for columns

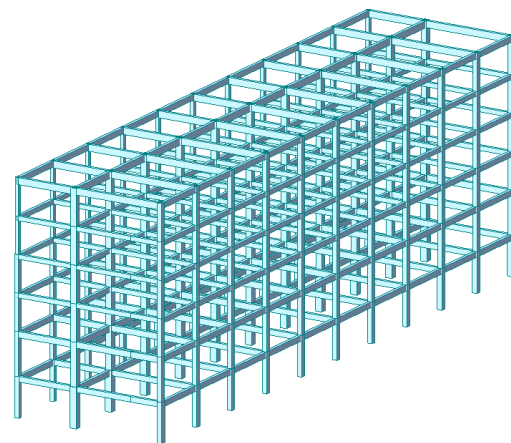
### 3. Seismic performance of an example structure

#### 3.1 Description of the model structure

For validation of the hybrid damper developed in this study, an analysis model structure is designed using only dead load of 5 kN/m<sup>2</sup> and live load of 2.5 kN/m<sup>2</sup>. The analysis model structure is a 6-story reinforced concrete building structure which is composed of moment resisting frames in both directions. The structure has a rectangular plan shape with 6 m span length along the longitudinal direction and 5 m and 9 m span length along the transverse direction as shown in Fig. 6. The slabs are assumed to be rigid diaphragm and the strengths of reinforced concrete and re-bars are assumed to be 21 MPa and 400 MPa, respectively.

#### 3.2 Modeling for nonlinear analysis

The seismic performance of the model structure was evaluated using the seismic performance criteria of ASCE/SEI 41-13 (2013). The nonlinear bending moment vs. rotation relationships of columns were represented by



(b) 3-D view

Fig. 6 Analysis model structure

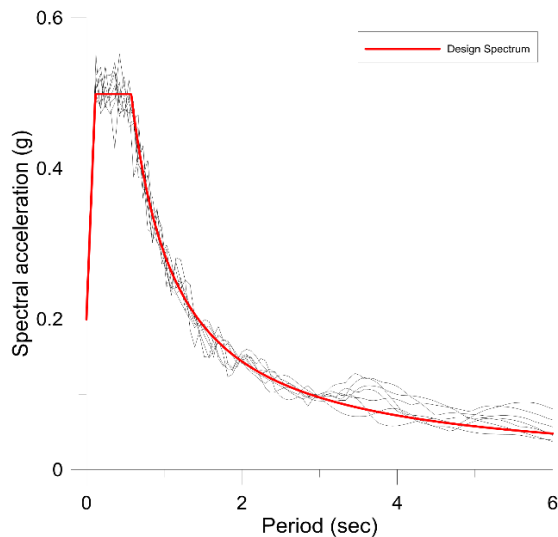


Fig. 8 Design spectrum and the response spectra of the earthquakes used in the analysis

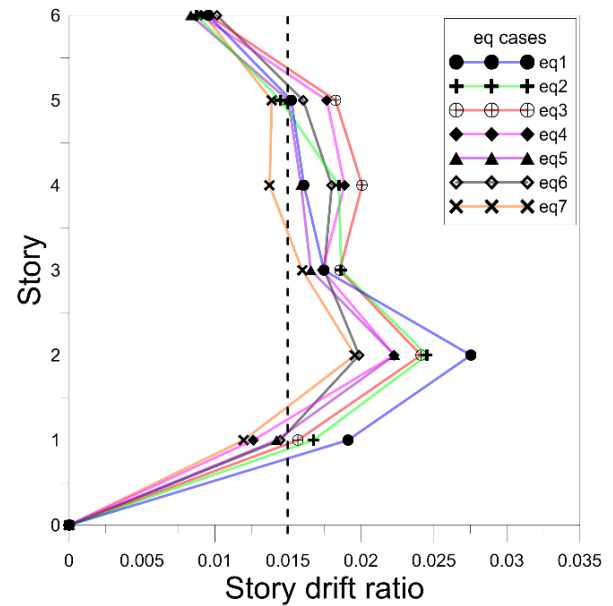


Fig. 9 Inter-story drift of the model structure subjected to the artificial ground motions along the transverse direction

tri-linear lines as shown in Fig. 8. The post yield stiffness varies depending on the axial force as specified in the ASCE/SEI 41-13. Following the recommendation of ASCE/SEI 41-13, the over-strength factors of 1.5 and 1.25 were applied for the strength of reinforced concrete and re-bars, respectively. Considering cracked section, the effective stiffness of the beams and columns in elastic range was reduced to  $0.5E_cI_c$  and  $0.7E_cI_g$ , respectively, where  $E_c$  is the concrete elastic modulus, and  $I_c$  and  $I_g$  are the second moment of inertia of the columns and girders, respectively. The shear strength of the elements was reduced to 40% of the uncracked sections. Nonlinear static and dynamic analyses were carried out using the program code Perform 3-D (2006). The hybrid damper was modeled using the 'Rubber Type Seismic Isolator Element' which can be used to model hysteretic damping devices as well as seismic isolators. The element has been successfully applied to model the behavior of slit dampers used for seismic retrofit of existing structures (Kim and Jeong 2016). Park *et al.* (2004) and Hessabi and Mercan (2016) showed that the stiffness of the structure which connects the damper to the structure may affect the effectiveness of the damping system. Therefore in this study it was assumed that the dampers are installed in the structure using steel trusses with stiffness significantly larger than that of the damper.

### 3.3 Nonlinear analysis of the model structure

To evaluate the seismic performance of the model structure, nonlinear dynamic analysis was carried out using the seven artificial earthquakes generated to fit the design spectrum constructed in the format of ASCE/SEI 7-13 (2013). The design spectrum was constructed using the spectral acceleration coefficients  $S_{DS}$  and  $S_{D1}$  equal to 0.50 g and 0.22 g, respectively. This corresponds to the seismic load with return period of approximately 1,000 years in Seoul area. In the construction of the design spectrum, the importance factor was assumed to be 1.2 and the response modification factor of 3.0 was used which corresponds to

the  $R$  factor for a RC ordinary moment frame. The design code requires that the structure should have seismic capacity satisfying the Life Safety limit state which is the maximum inter-story drift of 1.5% of the story height when the structure is subjected to a design level earthquake. Fig. 8 shows the design spectrum and the seven response spectra of the earthquakes generated using the design spectrum. Fig. 9 depicts the inter-story drift of the model structure subjected to the artificial ground motions along the transverse direction. It can be observed that the maximum inter-story drifts of the model structure along the transverse (short) direction exceed the limit state for all ground motions. As the structure satisfies the limit state along the longitudinal direction, seismic retrofit is conducted only along the transverse direction.

## 4. Optimum damper distribution scheme

In this section the hybrid dampers are distributed throughout the story for seismic retrofit of the model structure. An optimization technique named genetic algorithm (GA) is used for optimum design of dampers while the maximum inter-story drift is limited to 1.5% of the story height. Generations are reproduced by selecting individuals with good fitness which is determined by an objective function. In this study the damper distribution patterns which results in minimum total damper yield force (minimum initial cost) and minimum life cycle cost are chosen as the objective function. The Optimization Toolbox in MATLAB (2012) is used to run genetic algorithm.

In the first step of the optimum damper distribution process, a number between  $1 \sim (2^6 - 1)$  is randomly selected, where 6 is the number of story, and is changed to a binary number. Each string allocated with distinct binary number represents different damper distribution pattern. Next a

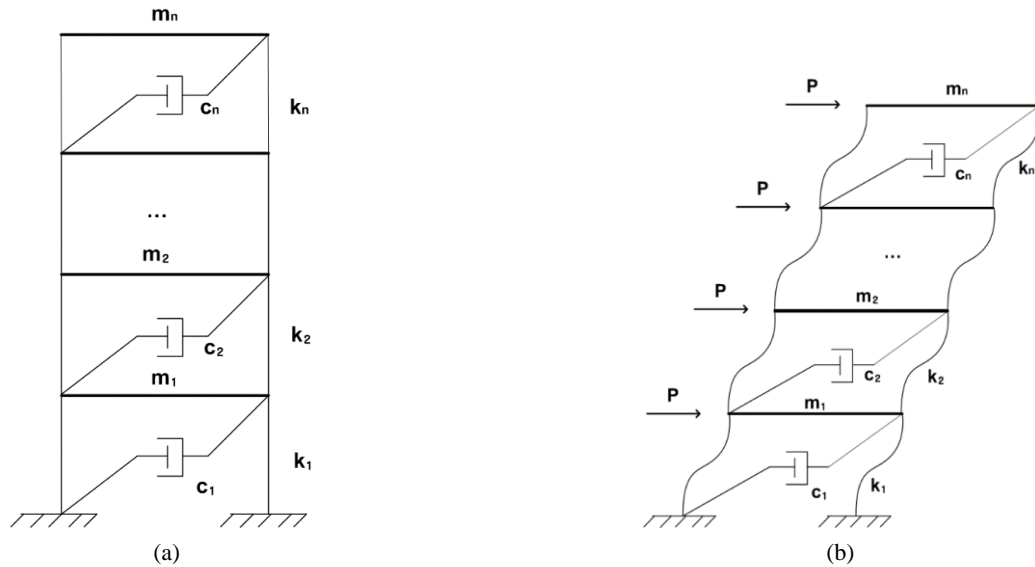


Fig. 10 Shear building approximation of the model structure

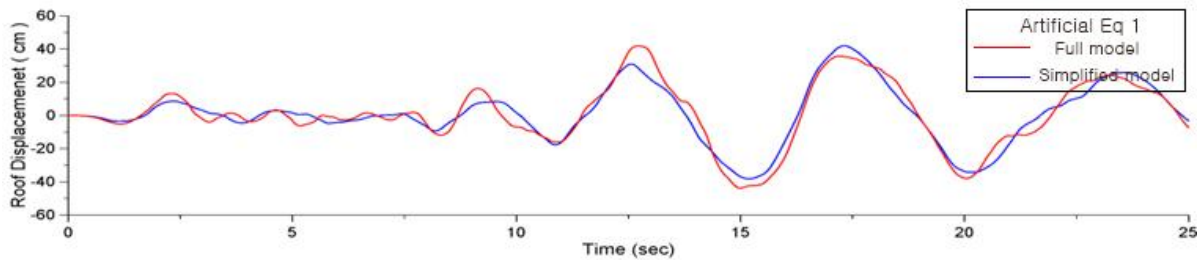


Fig. 11 Comparison of roof story displacement time histories obtained from analysis of full and simplified models

random damper yield force is assigned to the stories and the fitness value of each string of damper distribution is evaluated by nonlinear time history analysis of the model structure using an earthquake record. Then the second generation genes are reproduced from the parent genes using the roulette wheel selection method. Once two parent genes are selected by the roulette wheel selection method, some portion of their strings are switched to create two children genes which is called crossover. In this study the single point crossover operation is conducted 100 times to generate total of 100 second generation genes with the crossover rate of 50%. Next a string is randomly selected from the second generation genes and is mutated in such a way that each bit in the string is changed from 0 to 1 or vice versa. The process is repeated until an optimal value for design objective is reached. The maximum inter-story drift ratio is limited to 1.5% as constraints. The seismic performance of the structure for a specific damper distribution pattern is estimated by nonlinear analysis using seven artificial earthquake records generated previously.

Since huge number of nonlinear time history analyses are required in the optimization process using GA, the use of the full analysis model structure is not practical. To reduce the computation time significantly, the model structure was transformed into an equivalent 6 degrees of freedom system as shown in Fig. 10. The initial and post-yield stiffness of each story of the equivalent structure were

obtained from the story shear vs. inter-story drift relationships of the original structure obtained from pushover analysis. The stiffness matrix was scaled in such a way that the fundamental natural period of the equivalent structure becomes equal to that of the original structure. Fig. 11 depicts the roof story displacement time histories obtained from analysis of full and simplified models subjected to one of the artificial ground acceleration records. It can be observed that, even though there is slight difference locally, the general configurations of the two displacement time history curves coincide quite well.

In the optimization process hybrid dampers with uniform yield strength of 50 kN were used. Based on the preliminary analysis results, the ratio of the yield strength of friction and slit dampers was determined to be 1:9. Fig. 12 depicts the optimum damper distribution pattern obtained from GA in such a way that the total damper yield force becomes minimized. Total of 24 hybrid dampers were installed throughout the story. As the result slightly changes in each trial of the optimization algorithm, the mean values of the ten GA results are plotted in the figure. In each GA process, 1,000 story-wise damper distribution patterns (genes) were produced in each generation, and they were regenerated up to 100 times or until the change in the total damper yield force in each generation becomes very small. Mutation is made in 1% of the population in each generation.

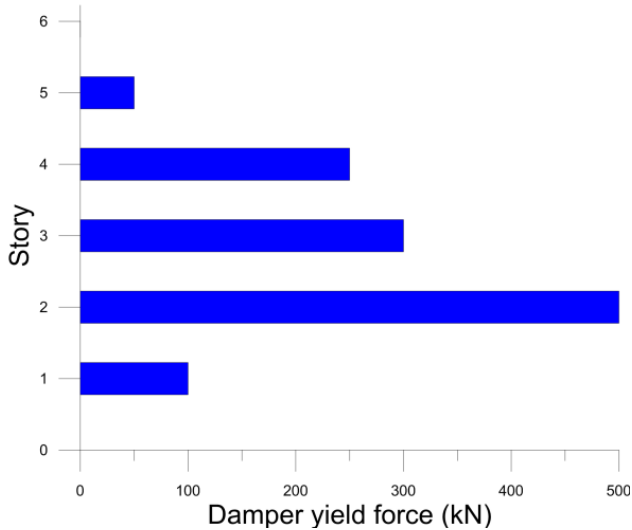


Fig. 12 Optimum damper distribution pattern minimizing total amount of dampers

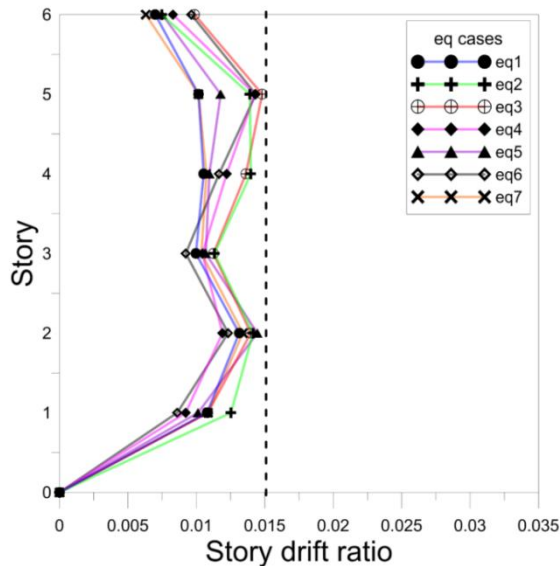


Fig. 13 Maximum inter-story drifts after seismic retrofit with optimally distributed dampers

Fig. 13 shows the maximum inter-story drifts of the model structure installed with optimally distributed hybrid dampers obtained from nonlinear dynamic analysis using the seven earthquake records. It can be observed that the maximum drifts are maintained within 1.5% of the story height as constrained in the optimization process. To confirm the validity of the optimization, the same amount of dampers were vertically distributed based on three intuitive methods such as (i) even distribution, distribution proportional to (ii) story shear and (iii) inter-story drifts. The results are plotted in Fig. 14 where it can be observed that the maximum inter-story drifts exceed 1.5% of the story height in every intuitive distribution case. This implies that, in order to satisfy the same limit state, more dampers are required in the intuitive methods which are generally applied in practice.

### 5. Life cycle cost evaluation procedure

To evaluate the seismic LCC of a structure, the probability of structural responses to exceed given limit states for the whole-life time of the structure needs to be evaluated. This requires the seismic hazard that a structure could experience throughout its lifetime, which is represented by the mean annual probability of exceedance for a spectral acceleration ( $S_a$ ) at the fundamental period of the structure. In this study three levels of seismic hazard, earthquakes with return period of 200, 1000, and 2400 years expected in Seoul area, were considered in the computation of seismic life cycle cost evaluation. Those three hazard levels match with the three performance levels or limit states defined in the guidelines of FEMA 356 such as Immediate Occupancy (IO), Life Safety (LS), and Collapse Prevention (CP) limit states, respectively.

The hazard function of spectral acceleration,  $H(s_a)$ , is the annual probability that intensity  $s_a$  at site will equal or exceed a specific response acceleration at a given response period  $s_a$ .

$$H(s_a) = P[S_a \geq s_a] = k_o s_a^{-k} \tag{3}$$

where  $k_o$  and  $k$  are the coefficients for linear regression of hazard  $H(s_a)$  on intensity  $S_a$  in proximity of limit state probability (region of interest) in logarithmic space.

Once the hazard and performance levels are defined, the probability of the structure to reach the pre-defined damage states throughout its lifetime needs to be computed to obtain the LCC of the structure. The fragility curve, which represents the probability of exceeding a pre-determined limit state ( $L_S$ ) for a certain seismic intensity, is constructed using the median,  $\lambda_D$ , and standard deviation,  $\tilde{\sigma}_D$ , of the maximum inter-story drift ratio (MIDR) obtained from nonlinear dynamic analyses of the model structure as follows (Aslani and Miranda 2005)

$$P(L_S|s_a) = \Phi \left[ \frac{\ln MIDR_{L_S} - \lambda_D}{\tilde{\sigma}_D} \right] \tag{4}$$

in which  $\Phi$  is the cumulative normal distribution function,  $\tilde{\sigma}_D$  is the logarithmic standard deviation of the MIDR evaluated at a given intensity measure  $S_a$ .

As the construction of fragility curve generally takes a lot of computational efforts, the time required for the optimization process can be significantly saved if the process can be simplified while the accuracy is maintained. For simplification of the fragility analysis, the probability  $P(L_S|s_a)$  of reaching a specific limit state for the 200 yr, 1000 yr, and 2500 yr hazards are determined first. Using these values, one can draw the fragility curve for 3 points only ( $P(L_S|s_a)$ ,  $S_a$ ). Assumption is made that the slope of fragility curve is constant around the  $P = 50\%$  based on the observation on the general shape of fragility curves for symmetric building structures. Then it is required to make curve fitting for 2 or 3 points to predict the near accurate location of  $P(L_S|s_a) = 50\%$  on the plot. From this simplification the spectral acceleration corresponding to the median drift capacity (i.e.,  $S_a^c$ ) can be easily obtained as done by Nour Eldin and Kim (2017).

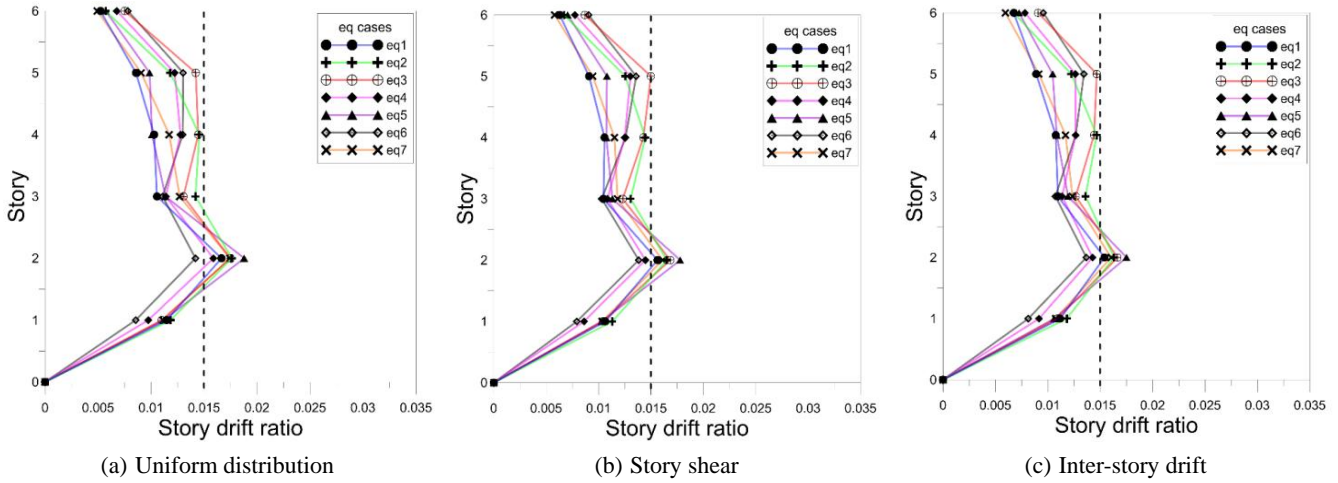


Fig. 14 Inter-story drifts of the structure retrofitted with dampers distributed by intuitive methods

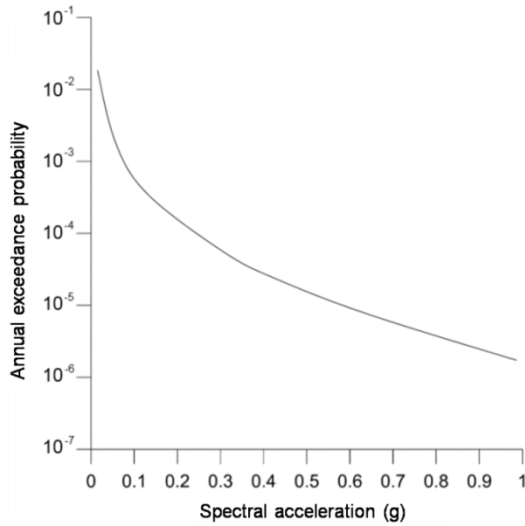


Fig. 15 Seismic hazard curve developed for Seoul area

Based on the seismic hazard and the fragility of the model structure, the expected LCC of a structure was calculated as (Genturck and Elnashai 2013)

$$E[C_{LC}] = C_o + \int_0^L E[C_{SD}] \left( \frac{1}{1+\lambda} \right)^t dt \quad (5)$$

$$= C_o + \alpha L E[C_{SD}]$$

where  $C_o$  is the initial construction cost,  $L$  is the service life of the structure, and  $\lambda$  is the annual discount rate. The annual expected seismic damage cost,  $E[C_{SD}]$ , is governed by a Poisson process (implicit in hazard modeling), hence does not depend on time; it is assumed that structural capacity does not degrade over time and the structure is restored to its original condition after each hazard; On the right hand side,  $\alpha$  is the discount factor equal to  $[1 - \exp(-qL) / qL]$ , where  $q = \ln(1 + \lambda)$ .  $E[C_{SD}]$  is given by

$$E[C_{SD}] = \sum_{i=1}^N C_i P_i \quad (6)$$

where  $N$  is the total number of limit-states considered,  $P_i$  is the total probability that the structure will be in the  $i$ th damage state throughout its lifetime, and  $C_i$  is the corresponding cost. In accordance with the definition of seismic hazard, three structural damage states were used (i.e.,  $N$  is equal to three): IO, LS and CP.  $C_i$  is assumed to be 30, 70 and 100 percent, respectively, of the initial cost of the structure. This is based on the correspondence of these damage states with the information provided by Fragiadakis *et al.* (2006).  $P_i$  is given by

$$P_i = P(\Delta_D > \Delta_{C,i}) - P(\Delta_D > \Delta_{C,i+1}) \quad (7)$$

where  $\Delta_D$  is the earthquake demand and  $\Delta_{C,i}$  is the structural capacity, usually in terms of drift ratio, defining the  $i$ th damage state. The probability of demand being greater than capacity  $\Delta_D > \Delta_{C,i}$  is  $P_{PL}$ , the damage state probability, which is the probability of the structure attaining the pre-defined damage states throughout its lifetime (annual probability of performance level not being met).

In its most basic formulation, damage probability can provide estimates of the annual probability of exceeding a selected performance level (PL), which can, in its simplest form, be determined as follows (Dolsek 2012)

$$P_{LS} = \int_0^{\infty} P(LS_{I_M=i_m}) \left| \frac{dH(i_m)}{di_m} \right| di_m \quad (8)$$

where the fragility  $P(\cdot)$  is the probability of exceeding a limit state if the intensity measure ( $I_M$ ) takes on a value equal to  $i_m$ , and  $H(i_m)$  is the hazard of the intensity measure. Cornell *et al.* (2002) have shown that the above equation can be approximated as follows

$$P_{LS} = H(S_a^c) \exp \left[ \frac{1}{2} \frac{k^2}{b^2} (\beta_D^2 |s_a + \beta_C^2) \right] \quad (9)$$

where  $P_{PL}$  is the damage state probability, the annual probability of performance level not being met;  $S_a^c$  is the spectral acceleration corresponding to the median drift capacity;  $H(\cdot)$  is the seismic hazard function of spectral

acceleration, annual probability that intensity  $S_a$  at site will equal or exceed  $S_a$ ,  $k$  is one of the coefficients for linear regression of hazard  $H(S_a)$  on intensity  $S_a$  in proximity of limit state probability (region of interest) in logarithmic space.  $b$  is one of the regression coefficients for linear regression of drift demand  $D$  on intensity  $S_a$  in logarithmic space;  $\beta_{D|S}$  is the dispersion measure for drift demand  $D$  at given  $S_a$ ;  $\beta_c$  is dispersion measure for drift capacity  $C$  (standard deviation of natural logarithm), assumed to be 0.3 based on previous studies (Cornell *et al.* 2002). Based on the maximum inter-story drift ratios obtained from nonlinear time history analysis of the model structure, the median ( $\mu$ ) and the standard deviation ( $\beta_{D|S_a}$ ) of the inter-story drifts can be evaluated. Then they can be used to calculate the probability, corresponding to each  $S_a^c$ , for each specific limit state

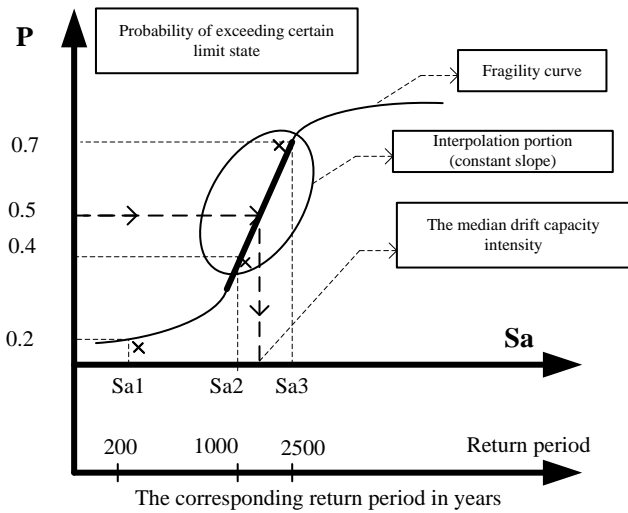


Fig. 16 Approximation of the fragility curve

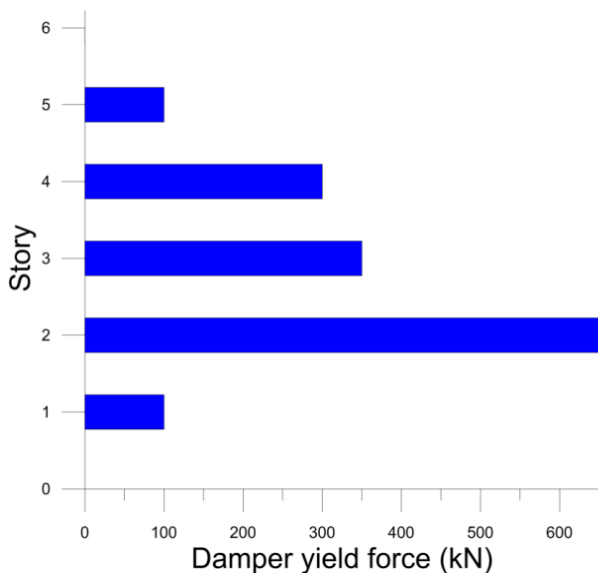


Fig. 17 Optimum damper distribution based on life cycle cost

### 6. Optimum damper distribution for minimizing life cycle cost

The next scheme for optimum seismic retrofit of the model structure was to locate the dampers in such a way that the life cycle cost (LCC), summation of initial retrofit cost and repair cost after earthquake, is minimized. To this end the simplified life cycle cost evaluation process described above was included in the optimization process. The cost of a hybrid damper unit including the connecting frame and installation cost such as chemical anchors and labor cost was estimated to be \$3,000. The structural material and construction costs were estimated based on the International construction market survey (2016) and RSMMeans Building Construction Cost Data (2014).

The inclusion of LCC in GA as an objective function further increase the computational demand significantly. In order to reduce the computation time to a practical range, the MDOF system of the original structure was transformed into an equivalent single degree of freedom (ESDOF) system for evaluation of LCC. For transformation, it was assumed that the response of the structure was dominated by the fundamental vibration mode. Pushover analysis was carried out using the lateral force proportional to the fundamental mode shape to obtain the capacity curve of the structure. The capacity curve was transformed to the force-displacement relationship of the ESDOF system, which was idealized to a bilinear line in such a way that the areas under the idealized and the capacity curves are equal. Detailed description for the transformation into an ESDOF system can be found in many references including Jeong and Elnashai (2007).

Fig. 17 plots the story-wise distribution of damper yield force obtained using genetic algorithm with the objective function of minimizing LCC. Average values over ten optimization results are presented in the figure. Total of 30 dampers with unit damper yield force of 50 kN are installed, which is more than the number of dampers

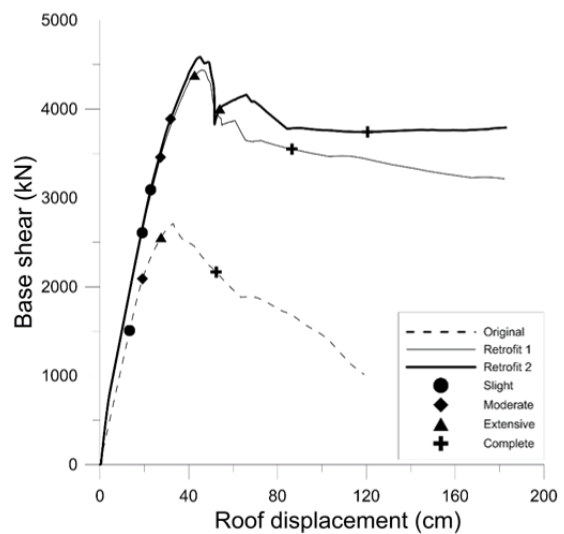
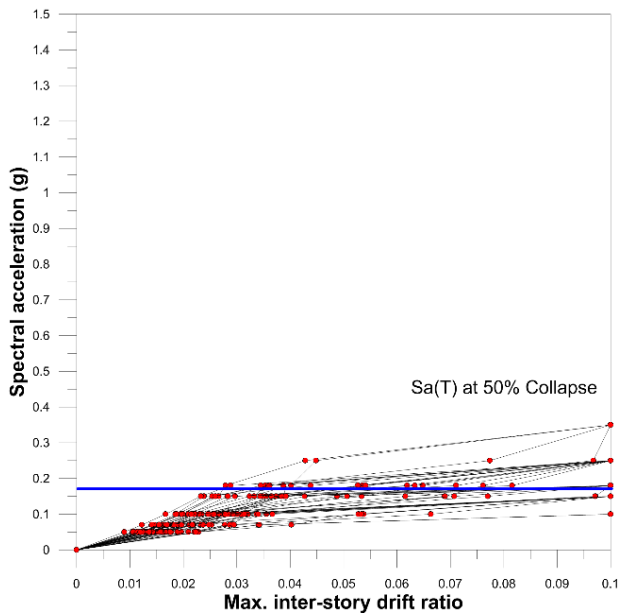


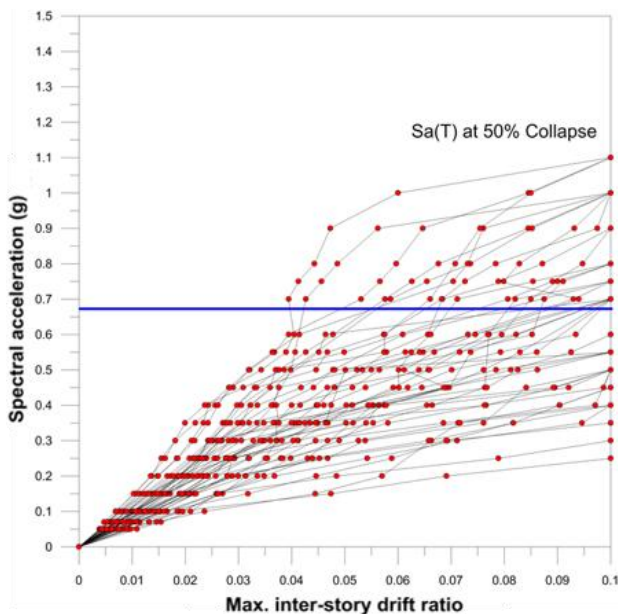
Fig. 18 Pushover curves of the model structure before and after seismic retrofit

installed by optimization with objective function of minimum damping force obtained previously

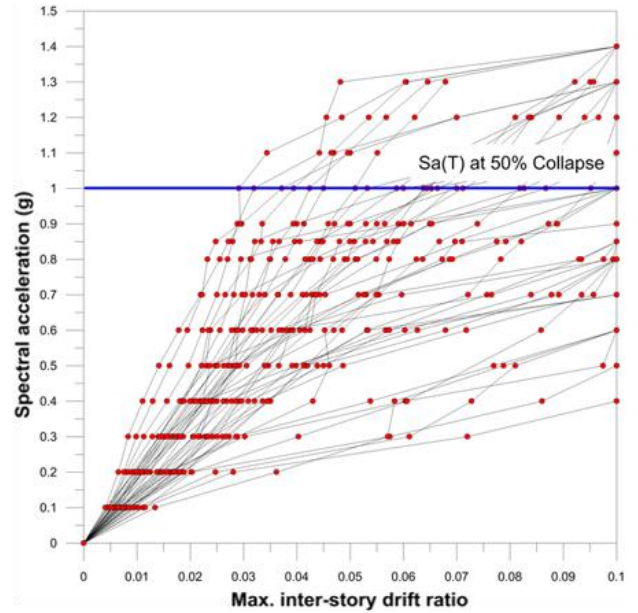
Fig. 18 depicts the pushover curves of the model structure before and after applying the two seismic retrofit schemes. The Retrofit 1 and Retrofit 2 represent the genetic algorithm-based retrofit schemes based on minimum damper yield force and LCC, respectively. The points of four damage states are indicated on the curves, which are Slight, Moderate, Extensive, and Complete damages as defined in HAZUS (2010). It can be observed that the overall strength of the model structure increases significantly after the retrofit. It also can be noticed that in the structure retrofitted based on LCC the Extensive and



(a) Original structure



(b) Structure with Retrofit 1



(c) Structure with Retrofit 2

Fig. 19 Continued

Complete damage states are reached at larger roof displacement.

The fragility analysis procedure was applied to the 3-D model structure to compare the probability of reaching a given limit state before and after retrofit with the hybrid dampers distributed with two different optimization schemes. Total of 44 far field seismic records provided in the PEER NGA database (2016) were used for fragility analysis. Nonlinear incremental dynamic analyses of the model structures were conducted using the ground motions to establish the median and the standard deviation of the collapse capacity of each analysis model. Fig. 19 depicts the spectral acceleration vs. maximum inter-story drift ratio curves obtained by incremental dynamic analyses of the model structures. From the incremental dynamic analysis results, the median capacities of the structures and their standard deviations were computed to be used for fragility analysis. From the figure it can be found that the median capacity of the original structure is 0.18 g, which is increased to 0.67 g and 1.0 g with application of the retrofit scheme 1 and 2, respectively.

Based on the incremental dynamic analysis results, the probability of reaching the four limit states and the corresponding fragility curves are drawn for the four different damage states in Fig. 20. It can be observed that the probabilities of reaching the damage criteria are largest in the original structure, and are smallest in the structures retrofitted with hybrid dampers distributed based on LCC. It can be observed that the difference in the failure probabilities of the structures retrofitted with the two optimization schemes becomes larger as the damage state changes from Slight to Complete damage. The spectral acceleration corresponding to the 50% probability of reaching the Moderate damage state increases from 0.03 g in the original structure to 0.12 g in the Retrofit 1 structure and to 0.26 g in the Retrofit 2 structure. The value increases

Fig. 19 Incremental dynamic analysis results of the model structures

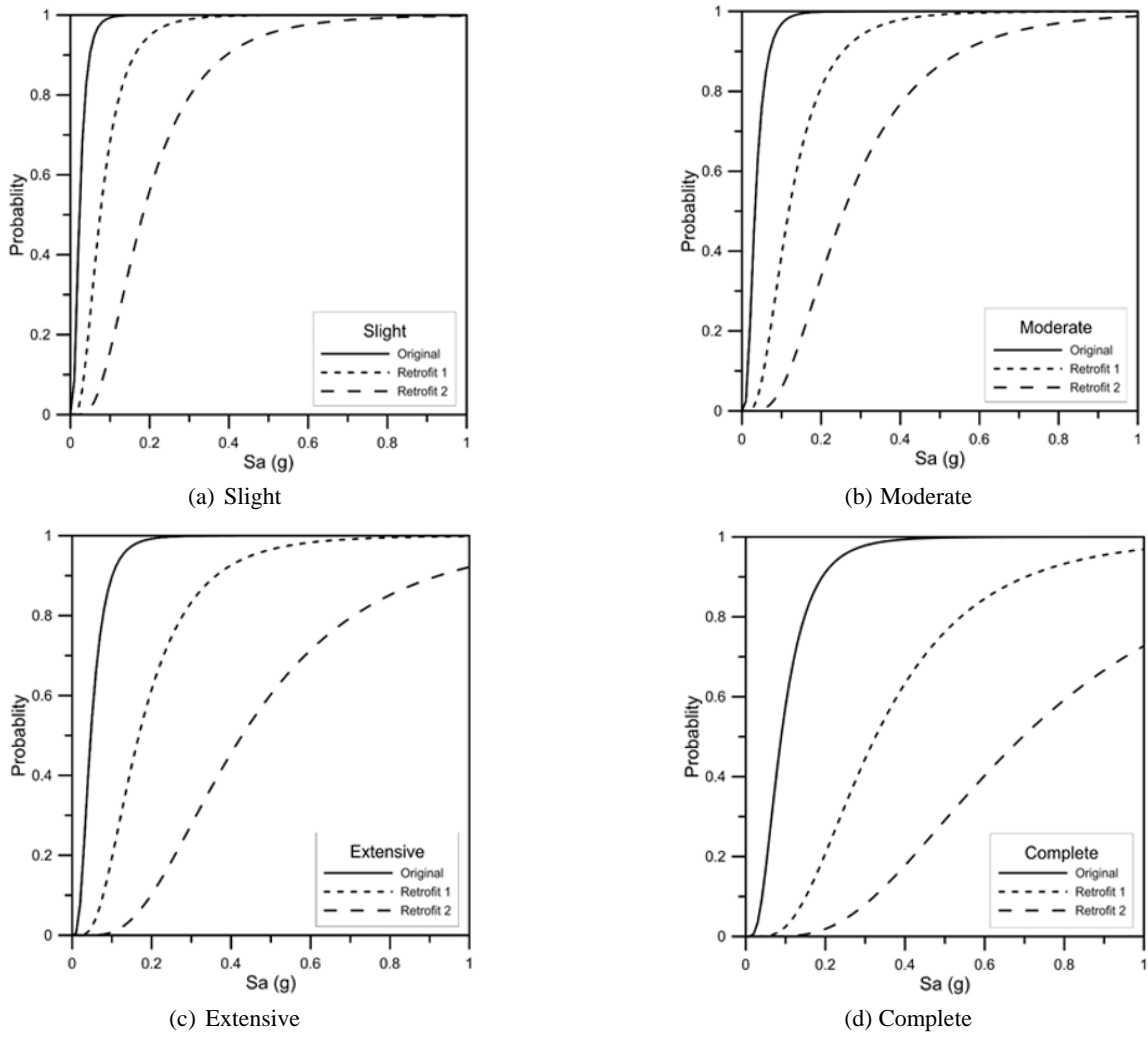


Fig. 20 Fragility curves of the model structure before and after seismic retrofit

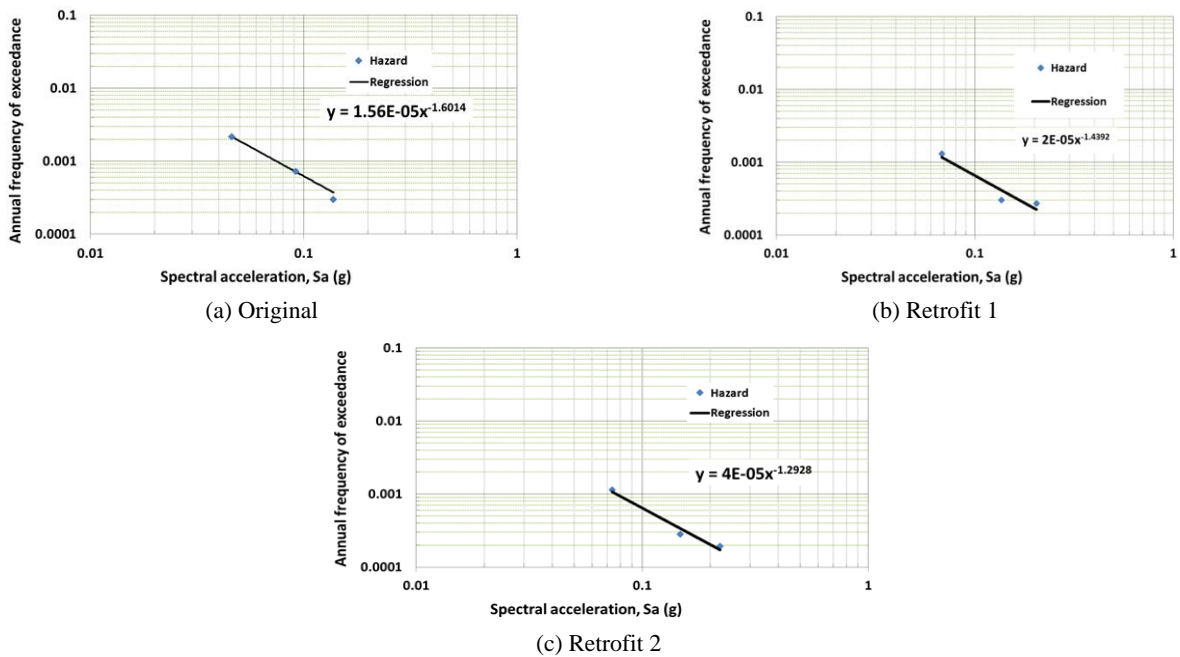


Fig. 21 Annual frequency of exceedance - spectral acceleration relationship of the model structure and regression curve to obtain  $k$  factor

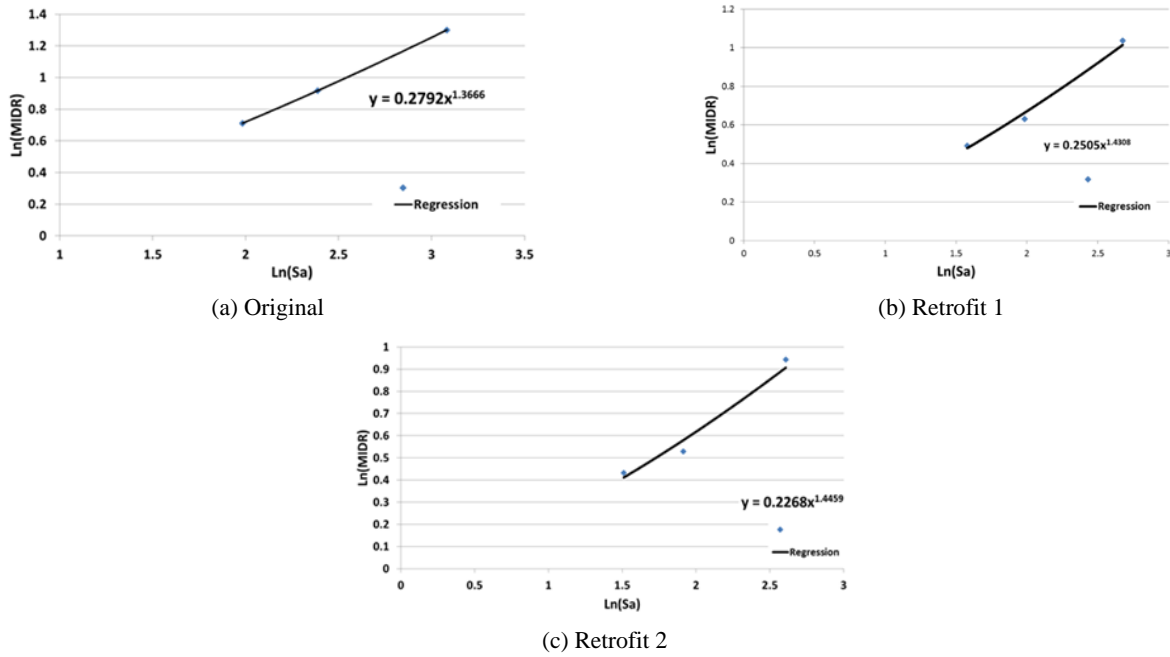


Fig. 22 Maximum inter-story drift-spectral acceleration relationship of the model structure and regression curve to obtain *b* factor

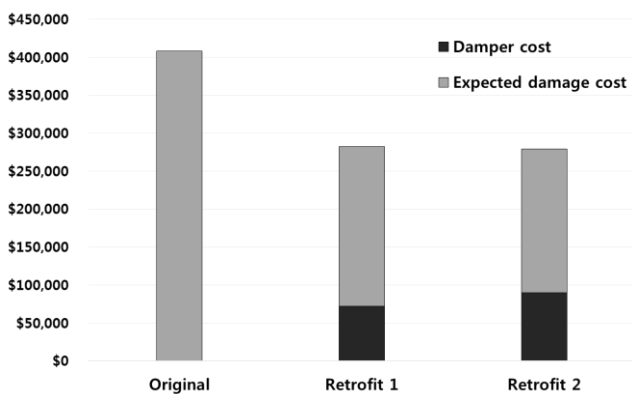


Fig. 23 Life cycle cost of the model structure before and after seismic retrofit

from 0.09 g in the original structure to 0.33 g and 0.70 g in the Retrofit 1 and Retrofit 2 structures, respectively. This implies that the LCC-based optimization scheme is more effective in enhancing seismic safety of structures subjected to medium to high earthquakes.

Fig. 21 shows the annual frequency of exceedance vs. spectral acceleration relationship of the 3-D model structure and the regression curve to obtain *k* factor in Eq. (3). Fig. 22 depicts the maximum inter-story drift vs. spectral acceleration relationship of the model structure and the regression curve to obtain *b* factor in Eq. (9). The seven artificial records generated above were used to obtain the analysis results. Fig. 23 shows the life cycle costs of the seismic retrofit of the model structure, which includes the cost for installation of dampers and repair cost after earthquake for the service life of 50 years. It is observed that the LCC of the original structure is \$408,145, which decreases to \$210,388 after seismic retrofit using the hybrid

dampers distributed for minimum damper yield force (Retrofit 1). The LCC further decreases to \$189,219 in the structure retrofitted with optimum damper placement based on LCC (Retrofit 2). The seismic retrofit scheme with higher initial cost but with smaller LCC confirms the validity of the optimum retrofit method based on LCC.

### 7. Conclusions

In this study the seismic performance of a hybrid damper composed of a steel slit plate and friction pads were evaluated, and the validity of optimum damper distribution schemes were investigated. A sample hybrid damper was tested under cyclic loading to confirm its effectiveness as a damping device and to construct its nonlinear analysis model. Genetic algorithm based optimization schemes were applied for optimum distribution of the dampers for seismic retrofit of a six-story framed structure. The validities of the optimum damper distribution schemes based on minimum initial cost and LCC were investigated by comparing the seismic fragility and the life cycle costs the of the model structure before and after the retrofit. The findings of the present study can be summarized as follows:

- The slit-friction hybrid damper developed in this study behaved stably throughout the loading history dissipating large amount of seismic energy.
- The analysis model structure retrofitted with the hybrid dampers turned out to satisfy the performance level given for the design basis earthquake.
- The simplification schemes for optimization and LCC estimation applied in this study were effective in reducing computation time significantly.
- The LCC-based optimization scheme turned out to be more effective than the initial cost optimization

scheme in minimizing the failure probability and LCC of the model structure, even though the initial cost of the former scheme is higher than that of the latter scheme.

- The hybrid dampers optimally distributed based on LCC proved to be more effective in enhancing seismic safety of structures subjected to medium to high earthquakes.
- The equivalent single degree of freedom approximation of the model structure and the simplified fragility analysis procedure were effective in the life cycle cost estimation of a structure for optimum damper distribution.

It should be pointed out that, as the optimization technique was verified using a 6-story moment frame structure, further verification would be necessary using structures with different dynamic characteristics. In addition, as this paper was focused on optimum distribution technique of dampers based on life cycle cost and the test was performed to obtain the analysis model of the proposed damper, further tests of the proposed dampers would be necessary to confirm the adequacy of the dampers on code specified requirements such as temperature and frequency dependency, resistance against wind load, etc., before they are applied in practice.

## Acknowledgments

This research was supported by Basic Science Research Program through the National Research Foundation of Korea (NRF) funded by the Ministry of Education (NRF-2017R1D1A1B03032809).

## References

- AISC 341-10 (2010), Seismic Provisions for Structural Steel Buildings; American Institute of Steel Construction, Chicago, IL, USA.
- ASCE/SEI 41-13 (2013), American Society of Civil Engineers; Seismic Evaluation and Retrofit of Existing Buildings, Reston, VA, USA.
- ASCE/SEI 7-13 (2013), American Society of Civil Engineers; Minimum Design Loads for Buildings and Other Structures: Reston, VA, USA.
- Aslani, H. and Miranda, E. (2005), "Probability-based seismic response analysis", *Eng. Struct.*, **27**, 1151-1163.
- Chan, R.W.K. and Albermani, F. (2008), "Experimental study of slit damper for passive energy dissipation", *Eng. Struct.*, **30**(4), 1058-1066.
- Cornell, C.A., Jalayer, F., Hamburger, R.O. and Foutch, D.A. (2002), "Probabilistic basis for the 2000 SAC Federal Emergency Management Agency steel moment frame guidelines", *J. Struct. Eng.*, **128**(4), 526-533.
- Dolsek, M. (2012), "Simplified method for seismic risk assessment of buildings with consideration of aleatory and epistemic uncertainty", *Struct. Infrastruct. Eng.*, **8**(10), 939-953.
- Fan, X.W., Xu, L.H. and Li, Z.X. (2017), "Behaviors comparisons and prediction of pre-pressed spring self-centering energy dissipation braces", *Int. J. Struct. Stab. Dyn.*, **18**(8), 1840006.
- FEMA (2012), Seismic Performance Assessment of Buildings: FEMA P-58, Prepared by the Applied Technology Council for the Federal Emergency Management Agency, Washington, D.C., USA.
- FEMA 461 (2007), Interim Testing Protocols for Determining the Seismic Performance Characteristics of Structural and Nonstructural Components; Applied Technology Council, Redwood City, CA, USA.
- Fragiadakis, M., Lagaros, N.D. and Papadrakakis, M. (2006), "Performance-based multi objective optimum design of steel structures considering life-cycle cost", *Struct. Multidiscip. Optimiz.*, **32**, 1-11.
- Gencturk, B. (2013), "Life-cycle cost assessment of RC and ECC frames using structural optimization", *Earthq. Eng. Struct. Dyn.*, **42**, 61-79.
- HAZUS-MH 2.1 (2010), Technical Manual; Federal Emergency Management Agency, Washington, D.C., USA.
- Hessabi, R.M. and Mercan, O. (2016), "Investigations of the application of gyro-mass dampers with various types of supplemental dampers for vibration control of building structures", *Eng. Struct.*, **126**, 174-186.
- Hessabi, R.M., Mercan, O. and Ozturk, B. (2017), "Exploring the effects of tuned mass dampers on the seismic performance of structures with nonlinear base isolation systems", *Earthq. Struct., Int. J.*, **12**(3), 285-296.
- International Construction Market Survey (2016), Turner & Townsend.
- Jeong, S. and Elnashai, A.S. (2007), "Probabilistic fragility analysis parameterized by fundamental response quantities", *Eng. Struct.*, **29**(6), 1238-1251.
- Karunaratne, N., Thambiratnam, D.P. and Perera, N.J. (2016), "Magneto-rheological and passive damper combinations for seismic mitigation of building structures", *Earthq. Struct., Int. J.*, **11**(6), 1001-1025.
- Kim, J. and Jeong, J. (2016), "Seismic retrofit of asymmetric structures using steel plate slit dampers", *J. Constr. Steel Res.*, **120**, 232-244.
- Kim, J. and Shin, H. (2017), "Seismic loss assessment of a structure retrofitted with slit-friction hybrid dampers", *Eng. Struct.*, **130**, 336-350.
- Lee, J. and Kim, J. (2015), "Seismic performance evaluation of moment frames with slit-friction hybrid dampers", *Earthq. Struct., Int. J.*, **9**(6), 1291-1311.
- Lee, C.H., Lho, S.H., Kim, D.H., Oh, J. and Ju, Y.K. (2016), "Hourglass-shaped strip damper subjected to monotonic and cyclic loadings", *Eng. Struct.*, **119**(15), 122-134.
- Lee, J., Kang, H. and Kim, J. (2017), "Seismic performance of steel plate slit-friction hybrid dampers", *J. Constr. Steel Res.*, **136**, 128-139.
- Marko, J., Thambiratnam, D. and Perera, N. (2004), "Influence of damping systems on building structures subject to seismic effects", *Eng. Struct.*, **26**(13), 1939-1956.
- Marshall, J.D. and Charney, F.A. (2012), "Seismic response of steel frame structures with hybrid passive control systems", *Earthquake Engineering and Structural Dynamics*, **41**(4), 715-733.
- MATLAB (2012), The MathWorks, Inc.; Natick, MA, USA.
- Murakami, Y., Noshi, K., Fujita, K., Tsuji, M. and Takewaki, I. (2013), "Simultaneous optimal damper placement using oil, hysteretic and inertial mass dampers", *Earthq. Struct., Int. J.*, **5**(3), 261-276.
- Nour Eldin, M. and Kim, J. (2017), "Simplified seismic life cycle cost estimation of a steel jacket offshore platform structure", *Struct. Infrastruct. Eng.*, **13**(8), 1027-1044.
- Park, J., Kim, J. and Min, K. (2004), "Optimal design of added viscoelastic dampers and supporting braces", *Earthq. Eng. Struct. Dyn.*, **33**, 465-484.
- PEER (2006), PEER NGA Database; Pacific Earthquake Engineering Research Center, University of California,

- Berkeley, CA, USA. URL: <http://peer.berkeley.edu/nga>
- Perform 3D (2006), Computer and Structures Inc.; PERFORM User Guide ver 4.
- Pinto, P.E., Giannini, R. and Franchin, P. (2007), "Seismic Reliability Analysis of Structures", *Earthq. Eng. & Struct. Dyn.*, **36**(13), p. 2081.
- RSMMeans Building Construction Cost Data (2014), Waier, Phillip R. (EDT).
- Sun, B., Wang, M. and Gao, L. (2017), "Design principles for stiffness-tandem energy dissipation coupling beam", *Smart Struct. Syst., Int. J.*, **20**(1), 53-60.
- Tsai, C.S., Chen, K.-C. and Chen, C.-S. (1998), "Seismic Resistibility of High-Rise Buildings with Combined Velocity-Dependent and Velocity-Independent Devices", *Proceedings of ASME Pressure Vessels and Piping Conference*, San Diego, CA, July, Volume 366, pp. 103-110.
- Uetani, K., Tsuji, M. and Takewaki, I. (2003), "Application of optimum design method to practical building frames with viscous dampers and hysteretic dampers", *Eng. Struct.*, **25**(5), 579-592.
- Whittaker, A.S., Bertero, V.V., Thompson, C.L. and Alonso, L.J. (1991), "Seismic testing of steel-plate energy dissipating devices", *Earthq. Spectra*, **7**(4), 563-604.
- Xu, Z., Zhao, H. and Li, A. (2004), "Optimal analysis and experimental study on structures with viscoelastic dampers", *J. Sound Vib.*, **273**(3), 607-618.
- Xu, Z., Tu, Q. and Guo, Y. (2012), "Experimental study on vertical performance of multi-dimensional earthquake isolation and mitigation devices for long-span reticulated structures", *J. Vib. Control*, **18**(13), 1971-1985.
- Xu, Z., Xu, F. and Chen, X. (2016), "Study on intelligent vibration isolation and mitigation of the platform by using MR and VE devices", *J. Aerosp. Eng.*, **29**(4), 04016010.
- Xu, L.H., Fan, X.W. and Li, Z.X. (2017), "Cyclic behavior and failure mechanism of self-centering energy dissipation braces with pre-pressed combination disc springs", *Earthq. Eng. Struct. Dyn.*, **46**(7), 1065-1080.
- Zahrai, S.M., Moradi, A. and Moradi, M. (2015), "Using friction dampers in retrofitting a steel structure with masonry infill panels", *Steel Compos. Struct., Int. J.*, **19**(2), 309-325.
- Zhan, M., Wang, S., Yang, T., Liu, Y. and Yu, B. (2017), "Optimum design and vibration control of a space structure with the hybrid semi-active control devices", *Smart Struct. Syst., Int. J.*, **19**(4), 341-350.